Spectroscopy and near infra-red upconversion of Er^{3+}-doped TZNT glasses

K. Venkata Krishnaiah[a,b], J. Marques-Hueso[c], K. Suresh[a], G. Venkataiah[a], B.S. Richards[d,e] and C. K. Jayasankar[a,*]

[a]*Department of Physics, Sri Venkateswara University, Tirupati – 517 502, India.*

[b]*Present address: Department of Engineering Physics, École Polytechnique de Montréal, 6079, Station Centre-ville, Montréal H3C 3A7, Canada.*

[c]*Institute of Sensors, Signals and Systems & Institute of Photonics and Quantum Sciences, School of Engineering and Physical Sciences, Heriot-Watt University, Edinburgh, EH14 4AS, United Kingdom.*

[d]*Light Technology Institute (LTI), Karlsruhe Institute of Technology, Engesserstrasse 13, 76131 Karlsruhe, Germany.*

[e]*Institute of Microstructure Technology (IMT), Karlsruhe Institute of Technology, Hermann-von-Helmholtz-Platz 1, 76344 Eggenstein-Leopoldshafen, Germany.*

[*]*Corresponding author: ckjaya@yahoo.com*

Abstract

In this paper we report on the near infra-red (NIR) upconversion (UC) and spectroscopic properties of erbium (Er^{3+})-doped TeO_2-ZnO-Nb_2O_5-TiO_2 (TZNT) oxide glasses. Judd-Ofelt theory has been applied to investigate the intensity parameters (Ω_λ, λ = 2, 4 and 6) which are used to derive radiative properties of the fluorescent levels. The different glasses present high refractive indices, low dispersion and Abbe numbers, as determined by variable angle spectroscopic ellipsometry. Under 980 nm excitation, the NIR emission profile and full width at half maximum have been studied in a broad range of Er^{3+} concentrations (0.01-3.0 mol%). On the other side, NIR UC has been obtained by exciting at 1523 nm, showing an increase of the intensity with Er^{3+} ion density in the studied range. The decay curves of the $^4I_{13/2}$ level exhibit single exponential nature for all the different concentrations. The lifetime of the $^4I_{13/2}$ level has been found to decrease (3.73-1.20 ms) after an initial increase (3.65-3.73 ms) with increasing of Er^{3+} ion concentration. The TZNT samples show broadband UC emission at

1.0 μm, which match with the band gap of silicon. This reveals that the investigated glasses could find application in photonics, for example non-linear optics and photovoltaic's.

Key words: Erbium ion; Spectroscopic ellipsometry; Broad band luminescence; Near infra-red upconversion; Photovoltaics;

1. Introduction

Over the last few decades, Erbium (Er^{3+})-doped materials have been investigated for the development of multitude of applications, among them the optical amplifiers [1], fiber lasers [2], temperature sensors [3], waveguide amplifiers [4], laser induced cooling [5], frequency upconverters [6], as well as for improving the c-Si solar cells [7] by spectral conversion. The Er^{3+} emission at 1550 nm has been used as Er^{3+}-doped fiber amplifiers in telecommunication systems [8,9]. Meanwhile, Er^{3+} emits intense green and red emissions in the processes of either anti-Stokes upconversion (UC) or Stokes shifted photoluminescence for color display devices [10]. Both near-infrared (NIR) emission (at 1.5 μm) and UC (at 980 nm) processes have been enhanced by co-doping with ytterbium (Yb^{3+}) ions as they have higher absorption cross-section at 980 nm. Jha *et al.* [11] investigated a maximum relative amplification gain in the range of 50–100 nm for the tellurite based optical fibers at C-(1535 nm) and L-(1560 nm) bands of 1.3 dB/cm and 0.6 dB/cm, respectively. On the other side, Danilo Manzani *et al.* [12], reported a loss of 9.6 dB/m for Er^{3+}/Yb^{3+}-doped tellurite fiber. Still, there is a demand for new optical materials for the development of optical fibers which covers the above-mentioned properties with low loss, which is a challenging task. The present study could address the broadband luminescence at 1.0 μm and 1.5 μm of Er^{3+}-doped tellurite glasses.

Tellurite glasses have some special properties over other oxide glasses such as high transparency window (0.35–6 μm), high linear and non-linear refractive index (≥ 2), low

melting points (~ 800 ^{0}C), low phonon cut-off (700-800 cm^{-1}), high dielectric constant (~20), good glass stability, and high lanthanide ion solubility compared to the other oxide glasses. Perhaps, most importantly, tellurite glasses can be readily formed into fibres and waveguides [13]. Because of the low phonon cut-off exhibited by tellurite glasses, these are favoured as host materials for UC processes. Even though the best reported UC materials are crystals, it is realized that glasses provide easier synthesis and can be made into larger dimensions. Moreover, they have been investigated for ultra-wide-band fiber Raman amplifiers which cover the S-, C- and L-bands [14]. It is supposed that, these glasses, when doped with UC lanthanide (Ln^{3+}) ions, could harvest the lower energy photons that are not absorbed in photovoltaic applications, and giving rise to higher energy above-band gap photons [15]. So, for example, the UC emission at 1.0 μm has been utilized to improve the quantum efficiency of c-Si solar cells in the 1.5 μm range [15,16]. Zhang and Heo [17] investigated on the UC of Er^{3+} ion in Er^{3+}/Yb^{3+} co-doped oxyfluoride glasses under 1550 nm excitation, with the results that where the 980 nm emission intensity increases with increasing Yb^{3+} concentration (0.5 and 1.0 mol%) as well as heat treatment temperatures (420 °C, 440 °C, 460 °C, 480 °C and 500 °C for 10 h). Yousef *et al.* [18] explored on the optical and crystallization kinetics of the titanium–zinc–niobium–tellurium oxide glasses. Thereafter, no other studies were reported on the particular glass system and an attempt is made for the first time to investigate the optical and luminescence properties of Er^{3+}-doped TZNTEr glasses.

This paper focuses on the concentration dependant spectroscopic and NIR UC properties of Er^{3+}-doped tellurite glasses with an aim to be utilized for solar cell applications. Ellipsometric studies are performed on the samples and the refractive index and Abbe number are evaluated. Judd-Offelt parameters are investigated and used for the evaluation of radiative properties. The luminescence properties are derived from the emission spectra for the $^{4}I_{13/2}\rightarrow{}^{4}I_{15/2}$ transition. Decay curves are recorded for the $^{4}I_{13/2}$ level of Er^{3+} ion and their

lifetimes are estimated. The UC was measured by exciting at 1520 nm and a possible mechanism is proposed to explain the radiative and non-radiative processes.

2. Materials and methodology

High purity (99.9 %, Aldrich) reagents (TeO_2, Nb_2O_5, ZnO, TiO_2 and Er_2O_3) were mixed with the molar composition, $(75\text{-}x)TeO_2 – 15ZnO – 5Nb_2O_5 – 5TiO_2 – xEr_2O_3$, where x = 0.01, 0.1, 0.5, 1.0, 2.0 and 3.0 mol% and referred as TZNTEr001, TZNTEr01, TZNTEr05, TZNTEr10, TZNTEr20 and TZNTEr30, respectively. The fine powders were melted in a platinum crucible for 40 min at 900 ºC and the molten glass poured on to a pre-heated brass mold at 280 °C (glass transition temperature, T_g). The samples were annealed for 10 h at the same temperature to release thermal stress/strains and allowed to cool to room temperature. The samples were subsequently cut and polished (dimensions: 10×10×2 mm^3) with optical quality for the measurements.

The refractive indices have been acquired using a spectroscopic ellipsometer (VASE, J.A. Woollam, U.S.A). The ellipsometric variables (Ψ and Δ) have been measured at three different angles of incidence (55°, 65° and 75°) over 360-2000 nm spectral region. The optical modelling has been conducted using the VASE32 (J.A. Woollam, U.S.A.) software package. The Raman spectrum was measured for TZNTEr001 sample by using a Renishaw inVia Raman Microscope (U.S.A) upon excitation at 786 nm laser excitation. The optical absorption spectrum was recorded using a spectrophotometer (Perkin Elmer Lambda–950, U.S.A.) from the ultra-violet (UV) to the NIR region. The NIR UC emission was measured by exciting the samples with a tunable laser (HP-Agilent, 8168-F) at1523 nm and detected with extended red photomultiplier tube (PMT). The NIR emission (1400-1600 nm) was measured with InGaAs detector under 980 nm excitation from a diode laser. The decay curves were measured by exciting the samples with a 980 nm diode laser by monitoring the

1.5 µm emission and the signals were acquired by a digital oscilloscope (LeCroy 200 MHz Oscilloscope, U.S.A.).

3. Results and discussion

3.1. Raman analysis

The measured Raman spectrum of TZNTEr001 sample by exciting with 785 nm wavelength laser is shown in Figure 1. The Raman bands are observed at 1046, 896, 771, 676, 427 and 120 cm^{-1}. A low frequency band at around 120 cm^{-1} is due to the vibration of Bason peaks which are correlated with the collective motion of acoustic phonons of atoms in glass [19]. On the one hand a weak band at 427 cm^{-1} arises from the symmetrical stretching vibration of Te-O-Te bonds that are formed by corner sharing of (TeO_4), (TeO_{3+1}) polyhedra and TeO_3 units [20]. A weak band centered at 676 cm^{-1} is attributed to the axial symmetrical stretching modes of (Te_{ax}–O) of TeO_4 tetrahedral [21]. The band positioned at around 771 cm^{-1} is assigned to the $(Te_{eq}–O)_s$ and $(Te_{eq}–O)_s$ vibrational modes of TeO_{3+1} polyhedra or TeO_3 trigonal bipyramidal units. On the other hand, a most intense and sharp band centred at 896 cm^{-1} corresponds to the stretching vibrations of Nb-O bonds in NbO_6 octahedra [22]. The second intense band at 1046 cm^{-1} is attributed to the isolated TiO_4 groups [23], and it indicates the maximum phonon energy of the titled glasses.

3.2. Optical properties

The ellipsometric analysis consists of measuring the state of polarization of the light after reflection on the material surface. Ellipsometric results were improved by modelling with Cauchy's equation to identify the roughness of the sample surface. Figure 2 shows the comparison of the ellipometric variables (Ψ and Δ) from 360-2000 nm region at different angles of incidence for the 0.01 Er^{3+}-doped TZNT sample. The value of roughness is comparable with the reported lead-tellurite glasses [24]. The quality of the adjustment (mean

square error, MSE) is smaller than unity for all samples except for 0.1% Er^{3+} (MSE=1.008) and in all cases better than the TeO_2-WO_3-ZrO_2-Er_2O_3 (TWZEr) glasses [25].

Figure 3 shows the variation of refractive index with wavelength (360-2000 nm) for TZNT samples. The measurements show that the refractive index increases with increase in Er^{3+} concentration. Moreover, the samples present a high index of $n \sim 2$ in a large region of the spectrum. This produces a very small Abbe number as low as 20 (see Table 1). As observed from Table 1, the refractive index of the investigated glasses are lower than one of TeO_2–WO_3–PbO-La_2O_3 (2.123 at 632 nm) [24] glass and higher than TWZEr (2.065 at 632 nm) glasses [20]. On the other hand, the Abbe number has been found to be 20, which is higher than the one of reported TWZEr glass (16) [25]. The glass with high refractive index and low Abbe number has potential applications in non-linear optics, for example, optical Kerr effect [26].

The absorption coefficient of the 1.0 mol% Er^{3+} -doped TZNT glass is shown in Figure 4. Absorption bands and their peak positions are assigned based on the free-ion Hamiltonian model [27]. The peak absorption bands (in nanometers), their experimental f_{exp} and calculated f_{cal} oscillator strengths, have been obtained using the well-known expressions [28-31] and are shown in Table 2. The small value ($\pm 0.13 \times 10^{-6}$) of the root mean square (*r.m.s.)* deviation between the experimental and calculated oscillator strengths indicates a good agreement among them. The absorption band, $^4I_{15/2} \rightarrow {}^2H_{11/2}$ located at 521 nm is more intense than the other bands, so called as higher sensitive transition which sensitive to environment even small changes around the Ln^{3+} ions. It is remarkable the wide absorption band for $^4I_{13/2}$ in line with similar glasses like TWZEr [25], which is advantageous for some non-linear processes like UC [32].

Judd-Ofelt [28,29] intensity parameters have been evaluated from the experimental oscillator strengths of various absorption bands and refractive index of the glass. The values

here obtained are represented in Table 3 along with the reported ones for other systems [4,6,10,33-36]. The trend of the obtained JO parameters $\Omega_2>\Omega_4>\Omega_6$, indicates the existence of a high degree of covalency or/and asymmetry around the RE ions. The spectroscopic quality factor (χ) found to be 1.52 for TZNTEr10 glass, which is higher than TeO_2-ZnO-ZnF_2 (TZF16) [6], Na_2O-Nb_2O_5-TeO_2 (NNT) [10], TeO_2-ZnO-PbO-PbF_2-Na_2O (TZPPN) [34], TeO_2-BaF_2-Na_2O (TBNE-1e) [35], B_2O_3-ZnO-TeO_2 (1ErTB) [36] and lower than TeO_2-P_2O_5-Al_2O_3-La_2O_3 [4], TeO_2-ZnO-ZnF_2 (TZF35) [6], and TeO_2-ZnO-ZnF_2-Na_2O (ETZ) [33]. This is an important predictor for stimulated emission in a laser active medium [37], initially represented for Nd^{3+} ion [38] and later used for evaluating all of the lasing ions.

Radiative properties such as radiative transition probability (A_R), branching ratio (β_R) and radiative lifetimes (τ_R) of the luminescent levels were predicted by utilizing the Judd-Ofelt parameters and refractive index. Those values are represented for TZNTEr10 glass in Table 4. The predicted values of τ_R in TZNTEr glass decrease following the order of $^4I_{9/2}$ > $^4I_{11/2}$ > $^4I_{13/2}$ > $^4F_{9/2}$ > $^4S_{3/2}$. Table 5 compares the τ_R, fluorescence lifetime (τ_f) (detailed explanation in coming sections) and quantum efficiency (η) of the investigated glass and of other already reported [4,6,10,39,40]. Because A_R is related to refractive index of the glass [41], a higher refractive index presents higher transition probabilities and follows the trend $^4S_{3/2}$ > $^4F_{9/2}$ > $^4I_{13/2}$ > $^4I_{11/2}$ > $^4I_{9/2}$. The parameter β_R of the luminescence transitions characterizes the lasing power of the transitions. The values of β_R for the $^4I_{9/2}\rightarrow{}^4I_{15/2}$ and $^4I_{13/2}\rightarrow{}^4I_{15/2}$ transitions have been found to be 59% and 100%, for TZNTEr10 glass. The value of τ_R for the $^4I_{13/2}$ level have been found to be 5.30 ms and it is compared with 7.2 ms [4], 3.23 [6], 3.02 [10], 3.33 [39] and 3.7 [40] as reported for other Er^{3+}-doped systems in Table 5. The τ_R is higher than the TeO_2-P_2O_5-Al_2O_3-La_2O_3 [4], TZF16 [6], TZF35 [6], Na_2O–Nb_2O_5–TeO_2 [10], TeO_2-ZnO [39] and lower than $PbHPO_4$ [40] glasses. In contrast, the quantum efficiency, estimated via the τ_f/τ_R, decreases with increasing Er^{3+} concentration

for the $^4I_{13/2} \rightarrow {}^4I_{15/2}$ transition and is found to be 70% which is higher than the reported for TeO_2-P_2O_5-Al_2O_3-La_2O_3 (56%) [4], TeO_2-ZnO (66%) [39] and lower than in TZF16 (184%) [6], TZF35 (189%) [6], Na_2O–Nb_2O_5–TeO_2 (96%) [10], and $PbHPO_4$ (74%) [40] glasses.

3.3. Luminescence properties

The concentration dependence emission spectra for the $^4I_{13/2} \rightarrow {}^4I_{15/2}$ transition of Er^{3+}-doped TZNT glasses upon 980 nm laser excitation is shown in Figure 5. The emission intensity increases from 0.01 mol% up to 1.0 mol% and then decreases with increase in concentration due to concentration quenching, shown in inset of Figure 5. The quenching of the luminescence intensity may be assigned to a non-radiative energy transfer [39] and can be analyzed by the decay curves in the coming sections. On the other side, *FWHM* increases with increasing concentration due to inhomogeneous broadening, as it is presented in Table 6. This broadening of the emission band with concentration is also explained by other radiation trapping effects [25] in which the emission of the excited Er^{3+} ion is re-absorbed by the non-excited Er^{3+} ion, considering the $^4I_{13/2} \rightarrow {}^4I_{15/2}$ transition and the following emission. This phenomenon always occurs in a typical 3-level system whenever the absorption and emission spectra overlap with each other. The re-absorption is also responsible for a small difference between experimental and calculated optical transitions [42,43], since the calculations don't consider this parameter while the direct measurement has it into account. Hence, the theoretical calculations are slightly higher than the observed in optical systems, more remarkably in highly concentrated systems.

The most important parameter in an optical amplification process is the stimulated emission cross-section ($\sigma_{em}(\lambda)$). The $\sigma_{em}(\lambda)$ can be evaluated from the reciprocity method described by McCumber (McC) [44], which is free from re-absorption (radiation trapping), using the measured absorption cross-section (σ_{ab}),

$$\sigma_{em}(\lambda) = \sigma_{ab}(\lambda)\frac{Z_l}{Z_u}\exp\left(\frac{E_{ZL} - hc\lambda^{-1}}{kT}\right) \quad (1)$$

where Z_l and Z_u are the partial functions of the lower (ground) and upper (excited) levels, respectively, and E_{ZL} is the zero-line energy which is equal to the energy separation between the lowest Stark components of the upper and lower levels of the Er^{3+} ion. The *h* and *k* are the Planck's and Boltzmann's constants, respectively. The ratio of the partial functions Z_l/Z_u becomes the degeneracy weighing of the two states corresponding to the $^4I_{13/2} \rightarrow {}^4I_{15/2}$ absorption transitions and, since this ratio does not change significantly with the change of chemical compositions, thus it is equal to 7/8 at room temperature. The absorption cross-section (σ_{ab}) for the $^4I_{15/2} \rightarrow {}^4I_{13/2}$ transition of Er^{3+} ion can be obtained by using the following equation [30],

$$\sigma_{ab} = \frac{2.303 * OD}{C.l} \tag{2}$$

where *OD* is the optical density, *C* is the Er^{3+} ion concentration and *l* is the thickness of the glass sample. Figure 6 shows the absorption and emission cross-section spectra of TZNTEr10 glass. The $\sigma_{em}(\lambda)$ found to be as high as 11.96 × 10^{-21} cm^2 than the other reported glasses [4,6,10,40,41]. On the other hand, the FWHM is found to be higher than TeO_2-P_2O_5-Al_2O_3-La_2O_3 [4], $PbHPO_4$ [40] and lower than TeO_2-ZnO [39], TZF16 [6] and TZF35 [6] glasses. The figure-of-merit (the product of the stimulated emission cross-section and bandwidth) is higher than for other reported glasses [4,6,10,40] except for TeO_2-ZnO [39] glass. Assuming that the figure-of-merit for bandwidth is an indication of the achievable gain band, the values obtained for TZNTEr01 sample suggest that they are promising materials for broadband light sources.

3.4. Near infra-red upconversion

Figure 7 shows the NIR UC emission spectra for the $^4I_{9/2} \rightarrow {}^4I_{15/2}$ of Er^{3+}-doped glasses for various concentrations under 1523 nm excitation. The characteristic emission

bands of Er^{3+} ions centred at around 975 nm corresponds to the $^4I_{11/2} \rightarrow {}^4I_{15/2}$ transitions. It is interesting to note that the UC emission increases enormously with increase in Er^{3+} ion concentration (0.01-3.0 mol%) and no luminescence quenching (to be expected for higher concentration) was noticed in the investigated range of concentrations. The FWHM increases with increase in concentration and is represented in Table 6. These highly Er^{3+}-doped glasses could be useful for c-Si solar cell applications as they emit intense emission at 1.0 μm region. Moreover, they present a high refractive index that diminishes reflection losses when integrated with a silicon cell, and they show a broad absorption band at $^4I_{13/2}$, which is crucial for UC photovoltaic's (PV) [45].

The UC emission at 980 nm may be due to two-photon excitation process in which the electrons populate $^4I_{9/2}$ level when excitation at 1550 nm [46]. The minimum number of photons required for the 980 nm emission is two [47]. The UC process may also occur through ground state absorption (GSA) for $^4I_{15/2} \rightarrow {}^4I_{13/2}$ transition followed either by excited state absorption (ESA) for $^4I_{13/2} \rightarrow {}^4I_{11/2}$ or $^4I_{13/2} \rightarrow {}^4I_{9/2}$ transitions or energy transfer upconversion (ETU) for $^4I_{13/2} \rightarrow {}^4I_{9/2}$ [48, 49]. The ETU is a process that depends directly on the distance between the Er^{3+} ions. In highly doped hosts such as 20% Er^{3+}:NaYF4 the dominant mechanism is GSA/ESA [48] due to the proximity of sensitizer and activator. Because the samples under study have a maximum of 3 mol% Er^{3+} ions are then supposed to be far away of each other, the ETU mechanism is likely to be lowered in respect to the GSA/ESA. The same mechanism may also be expected in TZNTEr samples after 1523 nm laser excitation is shown in Figure 8.

3.5. Decay curve analysis

The decay curves of Er^{3+}-doped tellurite glasses for 1.5 μm emission upon 980 nm laser excitation are shown in Figure 9. The curves show evidence of single exponential nature

even at higher concentrations. From the decay curves, lifetime of the $^4I_{13/2}$ level is found to decrease with increasing concentration after an initial increase, having the longer lifetime for 0.1 mol%. The increase of lifetime at lower concentrations is due to radiation trapping [50] as well as occupation of different sites [31], while the decrease at higher concentrations is due to concentration quenching originated by the enhancement of non-radiative relaxation processes. The decrease in lifetime may be also due to energy migration among Er^{3+} ions followed by transfer to recombination centers and interaction between Er^{3+} ions and the glassy host defects [51]. The lifetime of TZNTEr01 sample (3.73 ms) is higher than the other reported [10,39,40] and lower than tellurite [4,6] glasses. It is remarkable that the luminescence intensity is higher for TZNTEr10 sample where as the lifetime is higher for TZNTEr01 sample. This discrepancy either may be due to increasing of energy transfer at higher Er^{3+} concentration or those are neglected at lower concentration.

Conclusion

The Er^{3+}-doped tellurite (TZNT) glasses have been synthesized and investigated their optical and upconversion properties. The refractive index and Abbe number have been measured from spectroscopic ellipsometry. The JO parameters have been investigated and used to predict the radiative properties of the luminescent levels of Er^{3+} ions for 1.0 mol% Er^{3+}-doped TZNTEr10 sample and are compared with experimental values for 1.5 μm emission. Decay curves for the $^4I_{13/2}$ level exhibit single exponential nature for all the concentrations and the lifetime drawn from the single exponential fit. Lifetime shortens from 3.72 to 1.20 ms with increase in concentration after an initial increase from 3.65 to 3.72 ms, showing the longest lifetime for 0.1 mol% Er^{3+}-doped TZNTEr01 sample. Near infra-red upconversion has been obtained by exciting at 1523 nm, has potential for application in PV's to improve the efficiency of c-Si solar cells by utilizing the 1.0 μm emission.

Acknowledgment

One of the authors CKJ is highly grateful to the DAE-BRNS, Government of India, for the award of the Mega Research Project No. 2009/34/36/BRNS/3174. The authors J. Marques-Hueso and B.S. Richards thank the Engineering and Physical Sciences Research Council (EPSRC) for funding through the project EP/1013245/1.

References

1. S. Tanabe, N. Sugimoto, S. Ito, T. Hanada, J. Lumin. 87-89 (2000) 670-672.
2. Zhi-Xu Jia, Chuan-Fei Yao, Zhe Kang, Guan-Shi Qin, Yasutake Ohishi, Wei-Ping Qin, J. Appl. Phys. 115 (2014) 223103-223103-5.
3. A. Pandeya, S. Soma, Vijay Kumar, Vinod Kumar, Kaushal Kumar, Vineet Kumar Rai, H.C. Swart, Sensors and Actuators B 202 (2014) 1305-1312.
4. P. Nandi, G. Jose, C. Jayakrishnan, S. Debbarma, K. Chalapathi, K. Alti, A.K. Dharmadhikari, J. A. Dharmadhikari, D. Mathur, Opt. Express 14 (2006) 12145-12150.
5. A.J. Garcia-Adeva, R. Balda, J. Fernandez, Opt. Mater. 31 (2009) 1075-1081.
6. A. Miguel, R. Morea, J. Gonzalo, M.A. Arriandiaga, J. Fernandez, R. Balda, J. Lumin. 140 (2013) 38-44.
7. A. Shalav, B.S. Richards, T. Trupke, K.W. Krämer H.U. Güdel, Appl. Phys. Lett. 86 (2005) 013505-013505-3.
8. A. Mori, Y. Ohishi, S. Sudo, Electron. Lett. 33 (1997) 863-864.
9. P. Joshi, S. Shen, A. Jha, J. Appl. Phys. 103 (2008) 083543-083543-7.
10. Hai Lin, Shibin Jiang, Jianfeng Wu, Feng Song, N. Peyghambarian, E.Y.B. Pun, J. Phys. D: Appl. Phys. 36 (2003) 812-817.
11. A. Jha, P. Joshi, S. Shen, L. Huang, J. Non-Cryst. Solids, 353 (2007) 1407-1413.

12. Danilo Manzani, Jefferson Luis Ferrari, Ferminio Cesar Polachini, Younes Messaddeq and Sidney Jose Lima Ribeiro, J. Mater. Chem. 22 (2012) 16540-16545.
13. Raouf A.H. El-Mallawan, Tellurite Glasses Handbook: Physical Properties and Data (2nd ed.), (2012).
14. A. Mori, H. Masuda, K. Shikano, M. Shimizu, J. Light. Tech. 21 (2003) 1300-1306.
15. Fang Yang, Chao Liu, Dong Wei, Yongsheng Chen, Jingxiao Lu, Shi-e Yang, Opt. Mater. 36 (2014) 1040-1049.
16. G.E. Arnaoutakis, J. Marques-Hueso, A. Ivaturi, K.W. Krämer, J.C. Goldschmidt, S. Fischer, B.S. Richards, Optics Express 22 (2014) A452-A464.
17. J. Zhang, J. Heo, J. Non-Cryst. Solids 383 (2014) 188-191.
18. E. Yousef, A. E. Al-Salami, A Salem, E R Shaaban, Phys. Scr. 83 (2011) 015704-7.
19. W. Guonian, D. Shixun, Z. Junjie, W. Lei, Y. Jianhu, J. Zhonghong, Spectrochimica Acta Part A, 64 (2006) 349-354.
20. V. Kamalakar, G. Upender, Ch. Ramesh, V. Chandra Mouli, Spectrochimica Acta Part A 89 (2012) 149–154
21. D. Yin, F. Yang, L. Wu, Y. Zhou, H. Zhou, X. Wang, J. Alloys Compoun. 618 (2015) 666 – 672
22. I. Kabalci, H. Gokce, Acta Physica Polonica A 125 (2014) 877-881.
23. L. Pavic, N. Narasimha Rao, A. Mogus – Milankovic, A. Santic, V.Ravi Kumar, M. Piasecki, I. V. Kityk, N. Veeraiah, Ceramics International 40 (2014) 5989–5996 *and references there-in*.
24. M. Reben, B. Burtan, J. Cisowski, J. Wasylak, Photon. Lett. Poland, 4 (2012) 149-151.
25. K. Venkata Krishnaiah, G. Venkataiah, J. Marques-Hueso, P. Dharmaiah, C.K. Jayasankar, B. S. Richards, Sci. Advan. Mater. 7 (2015) 345-353.

26. Hang Zhang, Zhiguang Zhou, Aoxiang Lin, Jun Cheng, Hui Liu, Jinhai Si, Feng Chen and Xun Hou. J. Opt., 14 (2012) 065201-6.
27. A. Renuka Devi, C. K. Jayasankar, J. Non-Cryst. Solids 197 (1996) 111-128.
28. B. R. Judd, Phys. Rev. 127 (1962) 750-761.
29. G. S. Ofelt, J. Chem. Phys. 37 (1962) 511-520.
30. C. Gorller-Walrand and K. Binnemans, "Spectral intensities of *f-f* transitions," in *Handbook on the Physics and Chemistry of Rare Earths*, K. A. Gschneidner, Jr., and L. Eyring, eds. (North-Holland, 1998), pp. 101–264.
31. P. Babu, H. J. Seo, K. H. Jang, R. Balakrishnaiah, C. K. Jayasankar, A. S. Joshi, J. Phys. Condens. Matter 17 (2005) 4859-4876.
32. S.K.W. MacDougall, A Ivaturi, J. Marques-Hueso, K.W. Krämer, B.S. Richards, Opt. Express 20 (2012) A879-A887.
33. V. Nazabal, S. Todoroki, S. Inoue, T. Matsumoto, S. Suehara, T. Hondo, T. Araki, T. Cardinal, J. Non-Cryst. Solids 326&327 (2003) 359-363.
34. K. Damak, E. Yousef, S. AlFaify, C. Rüssel, R. Maâlej, Opt. Mater. Exp. 4 (2014) 597-612.
35. Ruosong Wang, Xiangwei Meng, Feixiang Yin, Yan Feng, Guanshi Qin, Weiping Qin, Opt. Mater. Express 3 (2013) 1127-1136.
36. Zahra Ashur Said Mahraz, M.R. Sahar, S.K. Ghoshal, M. Reza Dousti, J. Lumin. 144 (2013) 139-145.
37. D.K. Sardar, C.C. Russell III, R.M. Yow, J. Appl. Phys. 95 (2004) 1180-1184.
38. X. Qiao, X. Fan, M. Wang, X. Zhang, Opt. Mater. 27 (2004) 597-603.
39. N. Jaba, H. BenMansour, A. Kanoun, A. Brenier, B. Champagnon, J. Lumin. 129 (2009) 270-276.

40. C.C. Santos, I. Guedes, C-K Loong, L.A. Boatner, A.L. Moura, M.T. de Araujo, C. Jacinto and M.V.D. Vermelho, J. Phys. D: Appl. Phys. 43 (2010) 025102-025102-8.
41. K. Venkata Krishnaiah, K. Upendra Kumar, C.K. Jayasankar, Mater. Express 3 (2013) 61-70.
42. A. Boccolini, J. Marques-Hueso, B.S. Richards, Opt. Lett. 39 (2014) 2904-2907.
43. A. Boccolini, J. Marques-Hueso, D. Chen, Y. Wang, B.S. Richards, Solar Energy Materials and Solar Cells 122 (2014) 8-14.
44. D.E. McCumber. Phys Rev 136 (1964) A954-A957.
45. J. Marques-Hueso, R. Peretti, R. Abargues, B.S. Richards, C. Seassal, J.P. Martinez-Pastor, Adv. Opt. Mater. 3 (2014) 568-574.
46. S.R. Johannsen, L.R. Lauridsen, B. Julsgaard, P.T. Neuvonen, S.K. Ram, A.N. Larsen, Thin Solid Films 550 (2014) 499-503.
47. H. Lian, Z. Hou, M. Shang, D. Geng, Y. Zhang, J. Lin, Energy 57 (2013) 270-283.
48. S.K.W. MacDougall, A. Ivaturi, J. Marques-Hueso, K.W. Krämer, B.S. Richards, Solar Energy Materials and Solar Cells 128 (2014) 18-26.
49. W. Shao, G. Chen, J. Damasco, X. Wang, A. Kachynski, T.Y. Ohulchanskyy, C. Yang, H. Ågren, P.N. Prasad, Opt. Lett. 39 (2014) 1386-1389.
50. S. Shen, A. Jha, Opt. Commun. 205 (2002) 101-105.
51. L.R.P. Kassab, L.C. Courrol, R. Seragioli, N.U. Wetter, S.H. Tatumi, L. Gomes, J. Non-Cryst. Solids 348, (2004) 94-97.

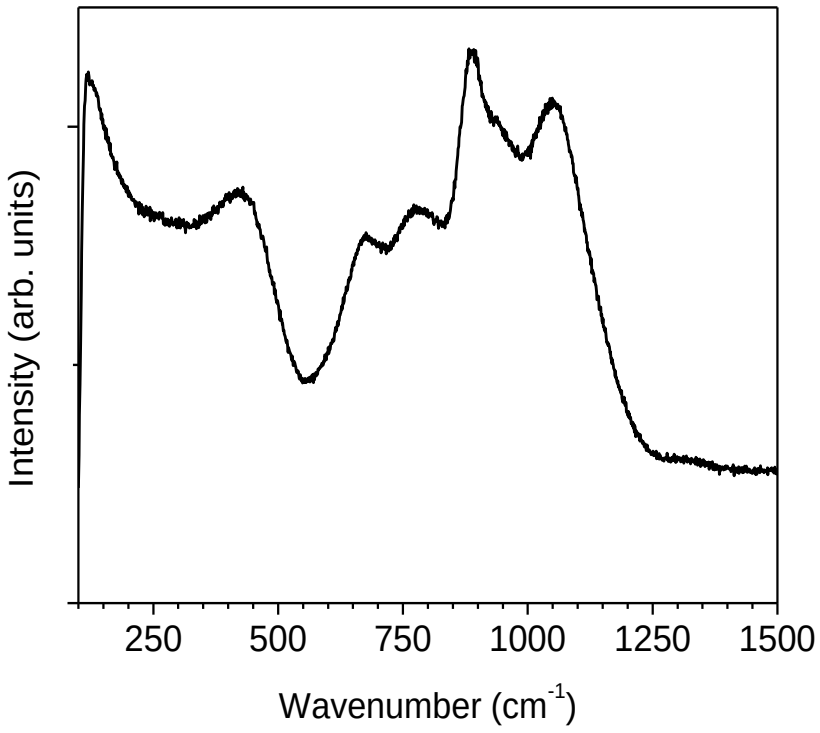

Fig. 1. Raman spectrum of TZNTEr001 sample upon excitation at 786 nm laser.

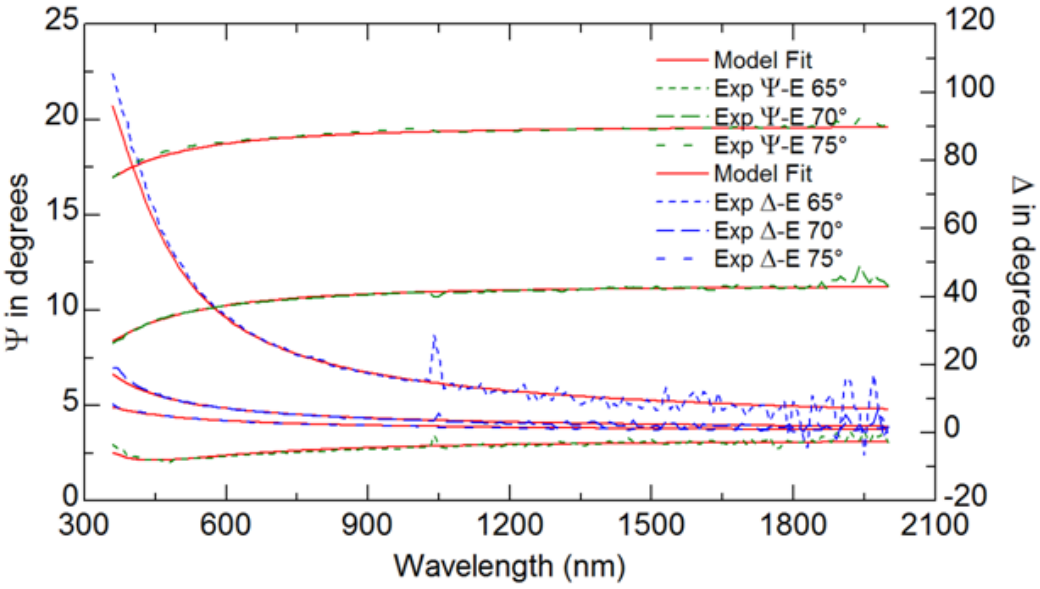

Fig. 2. Ellipsometric variables (Δ and Ψ) and model fit for the 0.01 mol% Er^{3+}-doped TZNT glass at different angle of incidence.

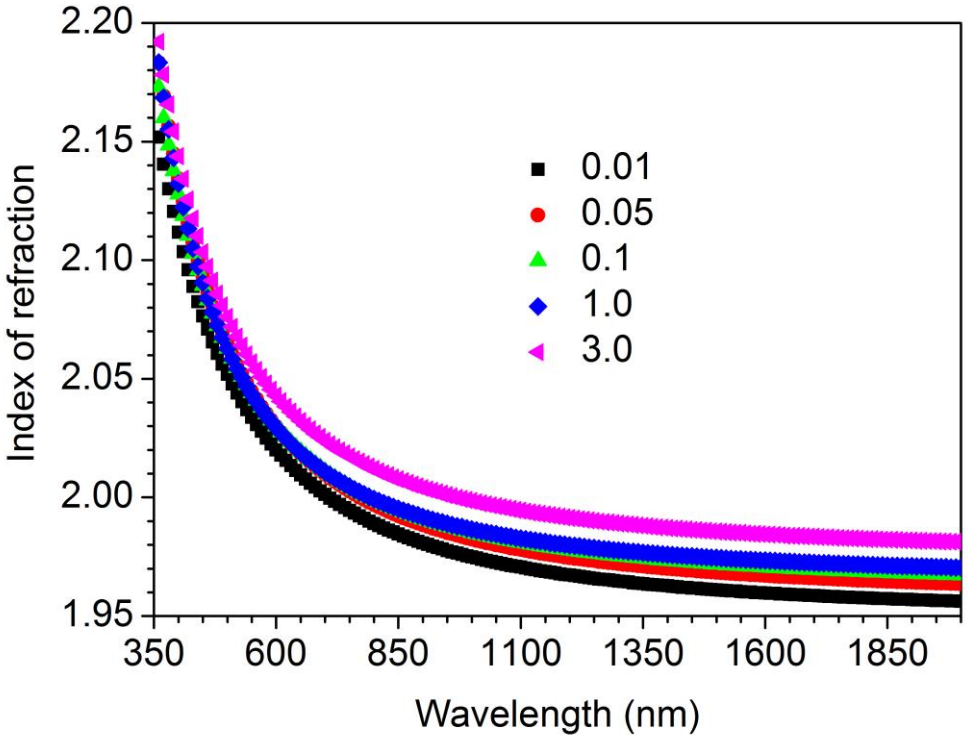

Fig. 3. Wavelength dependence of refractive index for different concentrations in TZNTEr glass.

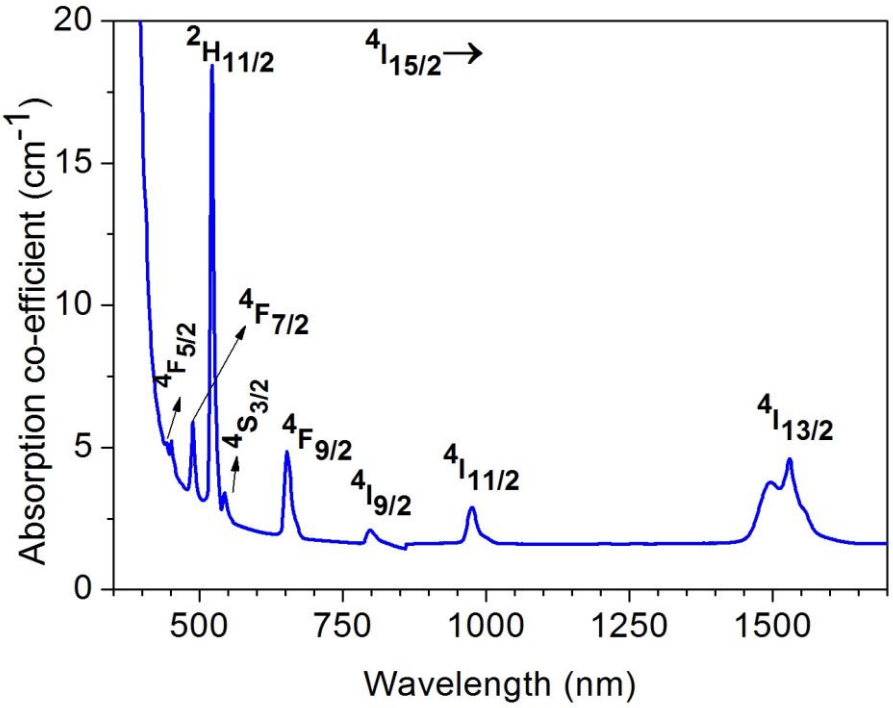

Fig. 4. Absorption spectrum of 1.0 mol % Er-doped TZNT glass in UV-visible-NIR region.

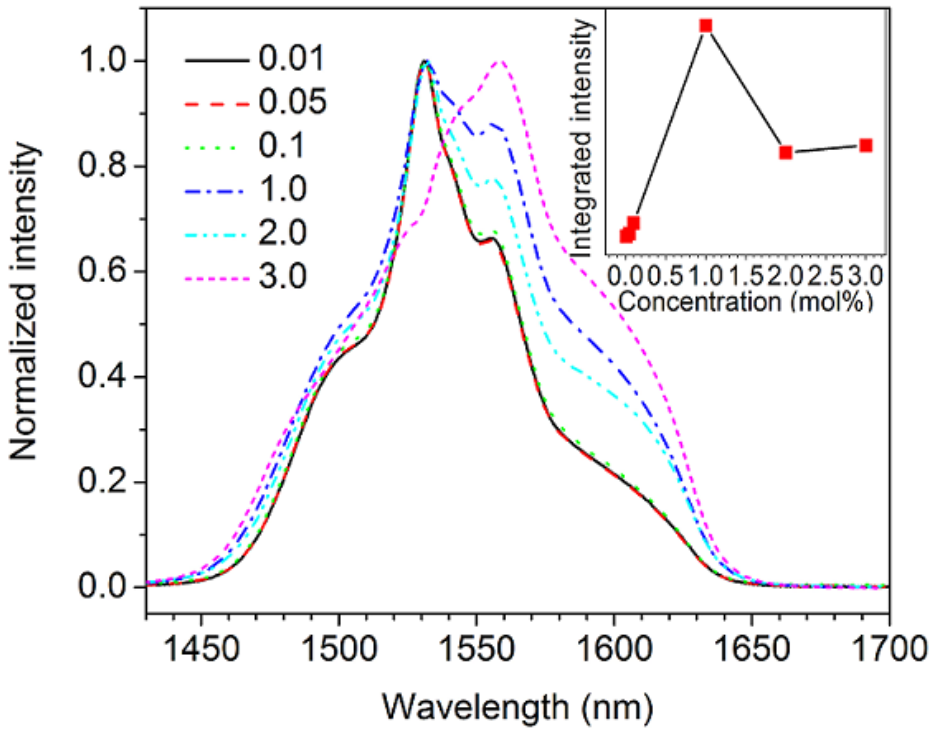

Fig. 5. Concentration dependence near infra-red emission spectra of TZNTEr glasses upon excitation at 980 nm laser.

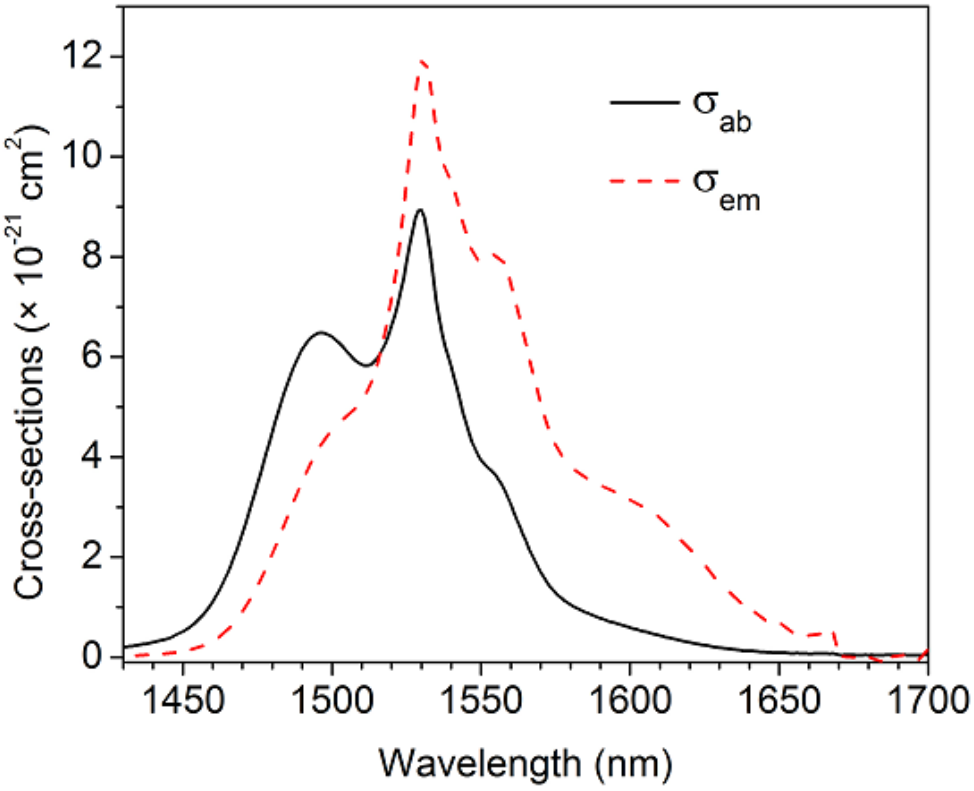

Fig. 6. Absorption and emission cross-sections of the $^4I_{13/2} \rightarrow {}^4I_{15/2}$ transitions for TZNTEr10 glass.

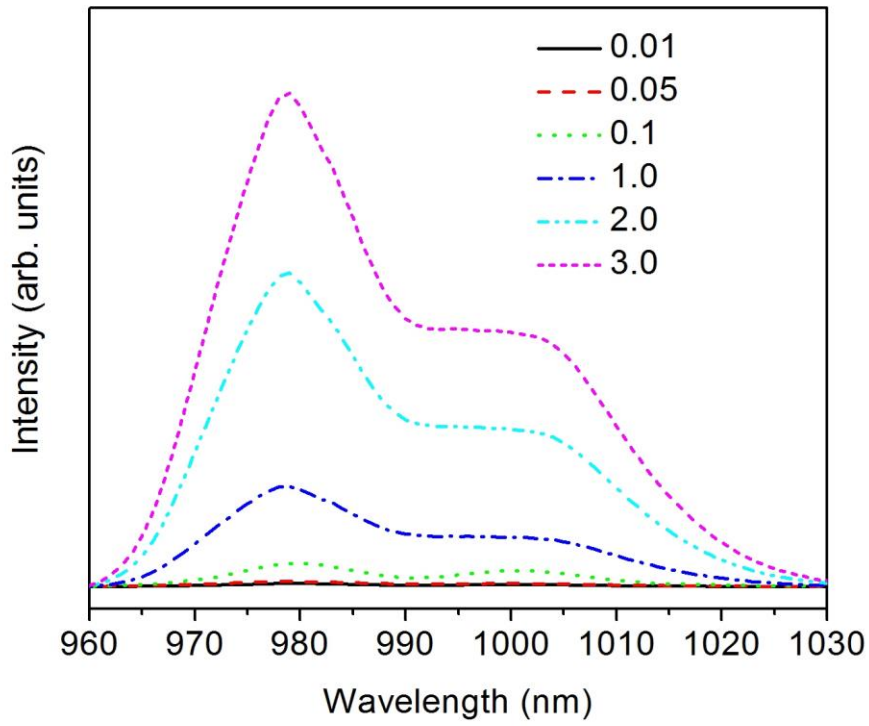

Fig. 7. Concentration dependence NIR UC spectra of Er^{3+}-doped TZNT glasses upon excitation at 1523 nm laser.

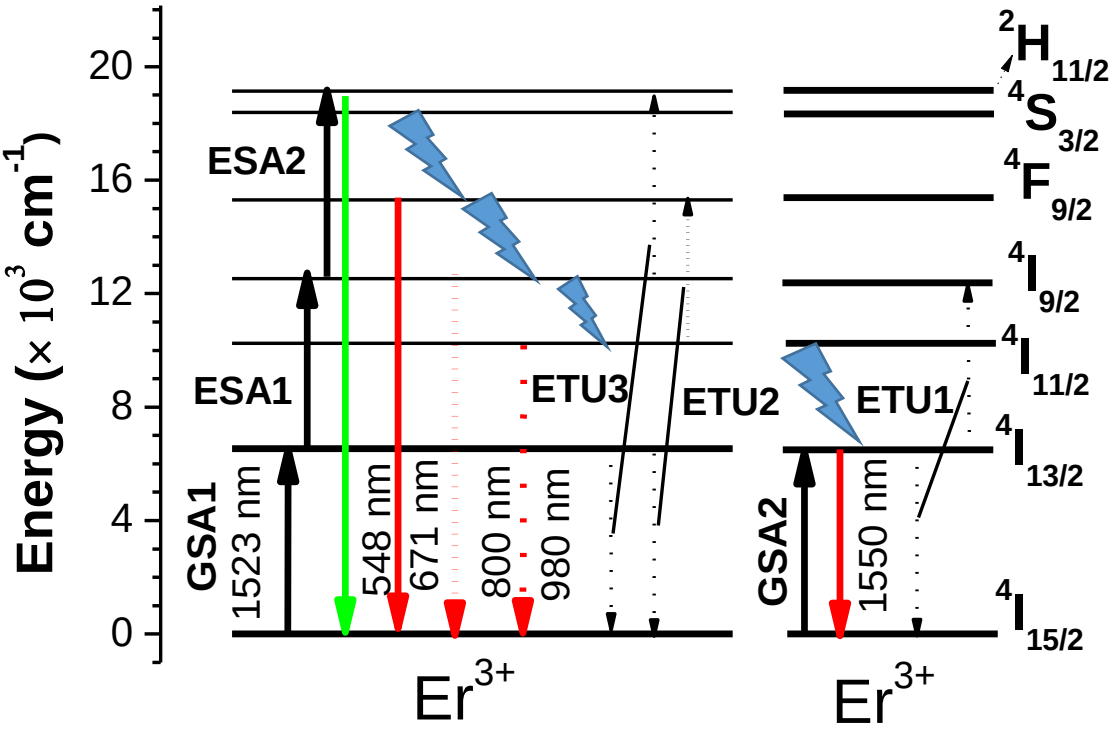

Fig. 8. Partial energy level diagram of Er^{3+} ions in TZNT glasses. Zig zag arrow represents the non-radiative transition.

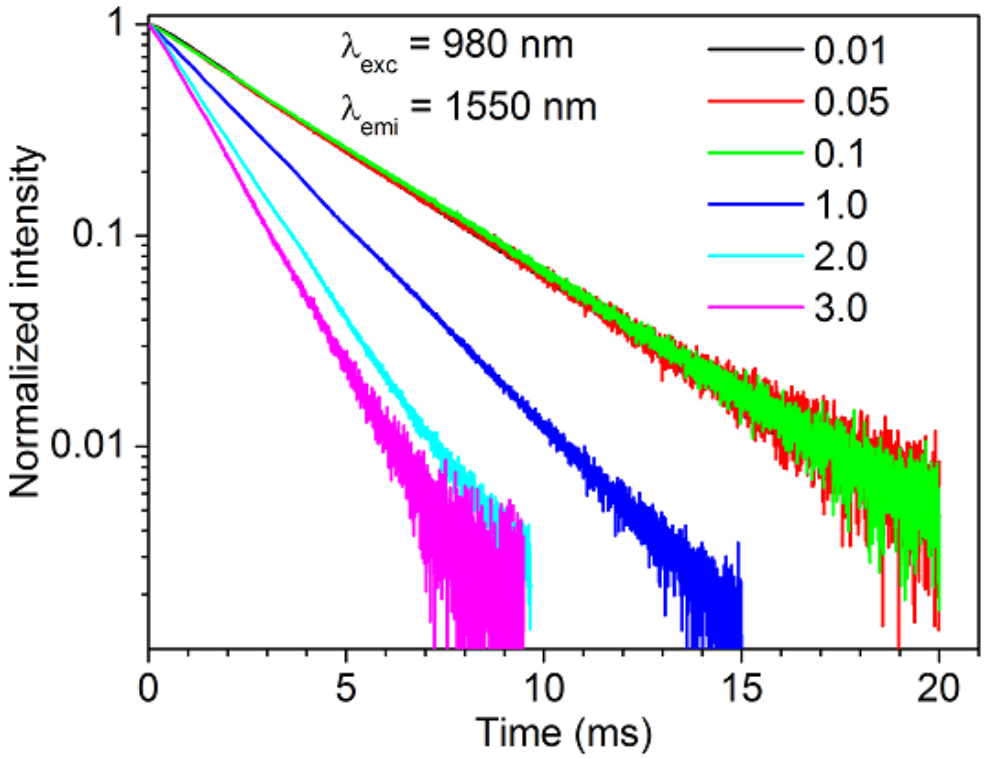

Fig. 9. Decay curves for the $^4I_{13/2}$ level of Er^{3+} ion at different concentrations.